IEEE Access
Multidisciplinary | Rapid Review | Open Access Journal

Received July 5, 2020, accepted July 16, 2020, date of publication July 20, 2020, date of current version August 5, 2020.

Digital Object Identifier 10.1109/ACCESS.2020.3010540

Hyper-Laplacian Regularized Non-Local Low-Rank Prior for Blind Image Deblurring

XIAOLE CHEN[1], RUIFENG YANG[1,2], CHENXIA GUO[1], SHUANGCHAO GE[1], ZHIHONG WU[1], AND XIBIN LIU[3]

[1]School of Instrument and Electronics, North University of China, Taiyuan 030051, China
[2]Automated Test Equipment and System Engineering Technology Research Center, Taiyuan 030051, China
[3]Unit 96901, People's Liberation Army of China, Beijing 100094, China

Corresponding author: Ruifeng Yang (yangruifeng@nuc.edu.cn)

This work was supported in part by the Scientific and Technological Innovation Programs of Higher Education Institutions in Shanxi, in part by the National Natural Science Foundation of China under Grant 41904080, and in part by the Key Research and Development Projects of Shanxi Province under Grant 201903D121118 and Grant 201903D121060.

ABSTRACT Blind deblurring of single image is a challenging image restoration problem. Recent various image priors have been successfully explored to solve this ill-posed problem. In this paper, based on the non-local self-similarity, we propose a novel method for blind image deblurring, which can simultaneously capture the intrinsic structure correlation and spatial sparsity of an image. Specifically, we use the hyper-Laplace prior to model the structure information of non-local similar patches, and embed it into the low-rank model as a smooth term of the energy equation. Since the established energy function is non-convex, an effective iterative optimization scheme is designed to effectively implement the proposed algorithm. In addition, we evaluate the proposed method for non-uniform deblurring problem. Extensive experimental results on both synthetic and real-world images show that the proposed method performs competitively against the state-of-the-art methods.

INDEX TERMS Blind deblurring, hyper-laplacian, non-local self-similarity, low-rank matrix approximation, non-uniform deblurring.

I. INTRODUCTION

As a basic image restoration technique, blind image deblurring is widely used in various image fields. The process of image blurring can be regarded as the operation of adding noise after convolution operation of blur kernel and original clear image, which can be modeled as

$$B = I \otimes k + n, \tag{1}$$

where B, I, k and n denote the observed blurred image, latent sharp image, blur kernel, and noise, respectively, and $\otimes$ represents convolution operator. It is a well-known ill-posed inverse problem to recover the clear image I and the corresponding blur kernel k rely on the blurred image B due to the non-uniqueness of solution.

To make this problem well-posed, additional constrains is required to regularize the solution space. Various methods based on the effective statistical prior from natural images have been successfully proposed for blind image deblurring. Numerous methods focus on the sparsity of image gradients [1]–[7], such as hyper-Laplacian prior [3], [4], total variation model [5], [6], normalized sparsity prior [7], L_0-regularized priors [12], [15]. Also, various statistical priors of natural image are explored, such as dark channel prior [16], extreme channels prior [18], local maximum gradient prior [40], Super-Gaussian Fields [29], MRF prior [45]. As all those priors are based on the assumption that coefficients in the gradient spaces are mutually independent, those approaches cannot model the complex structures of natural images. According to the fact that sharp edges are beneficial in the deblurring process, several blind deblurring methods exploit the structure of edges for kernel estimation [9], [19]–[24]. However, these methods are likely to fail when strong edges do not exist in blurred images.

Most of the above methods consider the relationship between adjacent pixel pairs or pixel intensity, while

The associate editor coordinating the review of this manuscript and approving it for publication was Mehul S. Raval.

ignoring the fact that complex structure of the real image depends on the connection between pixels in a larger range, and thus cannot effectively restore images with complex structures. In order to better solve the problem of image deblurring, patch-based priors were proposed and achieved excellent performance for restoring complex structures [13], [34], [50]–[53].

Motivated by the patch-based priors, in this paper, we propose a novel method from the perspective of structured information of non-local similar patches for blind image deblurring. Our method can not only model the complex structures of natural images, but also overcome the dependence on strong edges. Motivated by the observation that the distributions of singular values of the matrices formed by non-local similar patches are heavy-tailed [35], the hyper-Laplacian distribution is employed to deliver the intrinsic structure sparsity of non-local patches. Meanwhile, low-rank prior is adopted to characterize sparsity of the spatial domain. We then present a hyper-Laplacian regularized non-local low-rank approximation model, which can be formulated as an integration of the heavy-tailed distribution of non-local singular values and low-rank characteristics of non-local similar patches. By using an effective iterative optimization scheme, our algorithm shows the competitive performance on both synthetic datasets and real images. The main contributions of this work can be summarized as follows:

- We use the adaptive hyper-Laplacian distribution to depict rich structure information of non-local similar patches.
- By combining the heavy-tailed distribution of non-local singular values with low-rank characteristics of non-local similar patches, we propose an effective hyper-Laplacian regularized non-local low-rank matrix approximation model.
- An effective iterative optimization scheme based on half-quadratic splitting method is derived to solve the deblurring model. Experimental results on both synthetic datasets and real images demonstrated that the proposed algorithm performs competitive against the state-of-the-art methods.

II. RELATED WORK

Blind image deblurring has earned intensive attention in recent years. As blind image deblurring is an ill-posed optimization problem, additional constraints and prior knowledge are required to constrain the solution space. Fergus *et al*. [1] exploit characteristic of natural image gradient distribution and sparsity of blur kernel. It is shown in Levin *et al*. [3] that methods based on variational Bayesian inference perform better by removing trivial solutions compared to other methods with naive (maximum a posteriori) MAP formulations. To optimize the naive MAP framework, Levin *et al*. [4] adopt the hyper-Laplacian prior and develop an effective marginal approximation method for blur kernel estimation. Moreover, different likelihood functions and image priors have also been exploited to solve the ill-posed problem [2], [7]–[10], [12]–[16], [18]. Shan *et al*. [2] introduce a novel probabilistic model by using two piece-wise continuous functions to approximate the heavy-tailed natural image prior. Krishnan *et al*. [7] propose a normalized sparsity prior, i.e., L_1 / L_2 regularizer. Moreover, L_0 sparse representation is also developed. Xu *et al*. [12] and Pan and Su [14] employ L_0 sparse expression for kernel estimation. Pan *et al*. [15] apply L_0-regularized prior on intensity as well as gradient for text image deblurring task. In [16], dark channel prior is presented for blind image deblurring algorithm and achieves superior performance compared to other methods. However, dark channel prior based method is likely to fail in intermediate latent image estimation when the image contains a lot of bright pixels. Yan *et al*. [18] improve this method by incorporating dark channel prior with bright channel prior, which is named as extreme channels prior to achieve more efficient restorations. Unlike existing methods that use various priors to solve the deblurring problem, Pan *et al*. [32] explore the phase information in frequency domain to estimate accurate blur kernels and achieves competitive results.

Based on the idea that sharp edges which provide reliable edge information also make a great contribution to the constraint of solution space, some edge-based methods [19]–[21] have been proposed and achieve better performance on natural blurry images. Those edge-based methods depend on some heuristic strategy to select salient edges and remove tiny edges, thus leading to over-sharpening of image edges. Recently, Yang and Ji [24] proposed a novel variational expectation maximization method with built-in edge reweighting, which further prove the importance of edges for kernel estimation. However, strong structures do not always exist in blurred images.

Additionally, nonparametric regression is also used for image deblurring. Fergus *et al.* [1] propose a nonparametric estimator of blur kernel, which only impose some mild conditions rather than some prior information on the point spread function (psf). Kang *et al*. [49] also suggest a nonparametric method for estimating the psf without imposing any restrictive prior, because spatial blur will significantly affect the image structure near the edge, while in the continuous area of image intensity, the image structure will be less affected.

With the success of deep convolutional neural network (CNN) on image restoration problems, Li *et al*. [25] propose a discriminative prior which can be learned by a CNN classifier for deblurring task. Several learning-based methods [26]–[28] have also been proposed for blind image deblurring. However, it is difficult to synthesize realistic blurry images as the training dataset. Therefore, the performances of these methods will degrade on images with complex motion blurs.

Considering the relationship among similar patches, patch-based priors have been introduced to solve the problem of blind image restoration. Michaeli and Irani [13] propose patch recurrence prior for kernel estimation. Tang *et al*. [50]

employ external patch information and combine with sparse representation to guide the iteration of latent images. Guo and Ma [53] proposed an adaptive patch prior to recover low-level features. Xu *et al*. [51] develop a group sparse representation prior based on the observation that adjacent patches of the clear image have similar characteristics, whereas the corresponding patches of the blurred image do not.

Low rank matrix approximation (LRMA) methods, which based on non-local similar patches, have also been widely exploited in image restoration [30], [31]. Dong *et al*. [31] utilize low-rank prior in image denoising and performs well against existing methods. Dong *et al*. [17] propose a valid algorithm by making use of salient edges and low rank property of non-local similar groups. Ren *et al*. [34] introduce an enhanced low-rank prior for image deblurring based on the low-rankness of similar patches from both image intensity and gradient map. Xu *et al*. [52] propose a novel low-rank blind deblurring method that uses the weighted schatten p-norm minimization and L_0-regularized gradient prior. All these methods have made significant advances in blind image deblurring. In this work, we embed the heavy-tailed distribution of non-local singular values into low-rank prior for solving the blind image deblurring problem.

III. PROPOSED METHOD

In this section, we first analyze the problem formulation of low-rank matrix approximation based on the non-local self-similarity. Then we use the hyper-Laplace prior to model the structure information of non-local similar patches, and propose a hyper-Laplacian regularized non-local low-rank matrix approximation model for blind image deblurring.

A. NON-LOCAL LRMA

Low rank matrix approximation (LRMA) methods have shown great advantages for the intermediate latent image restoration. Under the observation that self-repeating patterns exist across the whole image matrix, the formed data matrix composed by similar patches exhibits low-rank property. To recover the desired low-rank approximation X from its observation matrix Y, previous works [11] solved this non-convex problem by using standard nuclear norm $\|\cdot\|_*$ as the convex surrogate of the rank, which penalize all the singular values equally. Gu *et al*. [37] propose a weighted nuclear norm minimization (WNNM) algorithm, which is described as

$$\min_X \|Y - X\|_F^2 + \|X\|_{\omega,*}, \tag{2}$$

where $\|X\|_{\omega,*} = \sum_i \omega_i \sigma_i(X)$ means the weighted nuclear norm of X, that is, the sum of singular values of matrix X. $\sigma_i(X)$ denotes the i-th singular value and $\omega = [\omega_1, \ldots, \omega_n]^T$ is the non-negative weights which is inversely proportional to $\sigma_i(X)$. As analyzed in [37], larger singular values gather more information and therefore should be shrunk less, which enhances the robustness of the nuclear norm and achieves excellent performance in numerous vision tasks.

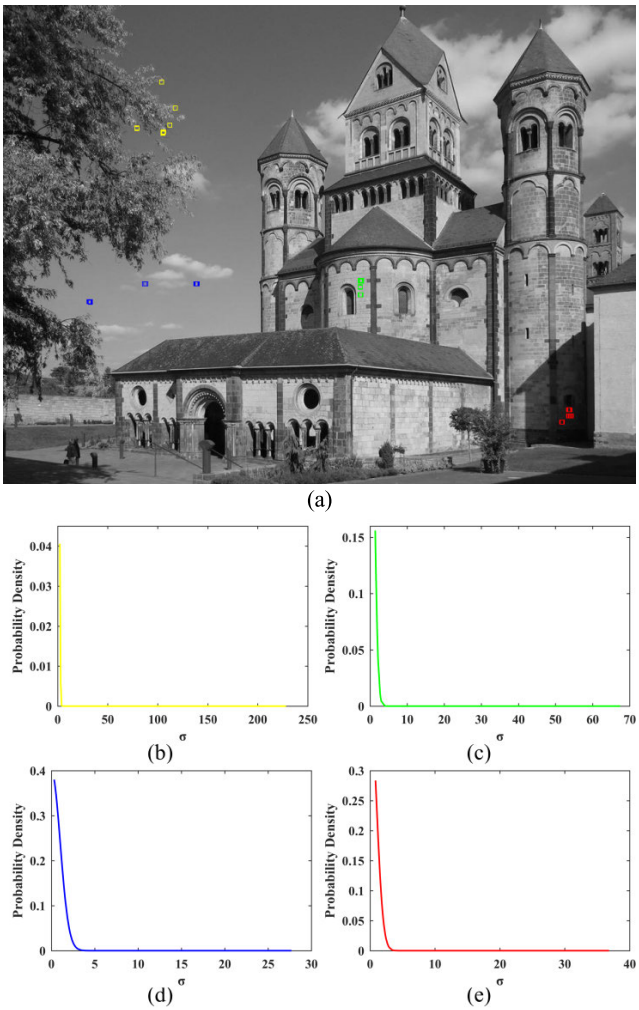

FIGURE 1. The empirical distributions of the non-local singular values of diffierent clusters which are labeled by yellow, blue, green and red, respectively. σ represents non-local singular value of the matrices formed by non-local similar patches. (a) Natural image. (b)–(e) Heavy-tailed distributions of the singular values of the matrices formed by non-local similar patches.

B. HYPER-LAPLACIAN REGULARIZED NON-LOCAL LRMA MODEL

Despite the great success of LRMA model in image restoration, most methods enforce sparsity constraints only across the spatial domain which cannot well describe the fine structures of natural images. One key observation of this work is that non-local singular values of the matrices formed by non-local similar patches are distributed with heavy-tails. Fig. 1 illustrates the empirical distributions of the non-local singular values of non-local matrices. The patch size is set as 7×7 pixels, and 60 non-local similar patches to a given patch are collected to form a 49×60 matrix. Then the singular values of the non-local matrix are calculated by Singular Value Decomposition (SVD).

From Fig. 1(b)–(e), we can see that non-local singular values are distributed with heavy-tails. Wang *et al*. [35] proposed a novel regularization of low-rank by parameterizing the heavy-tailed distribution of non-local singular values with generalized Gaussian distribution. Considering

the computational efficiency, we borrow a type of new heavy-tailed distribution termed hyper-Laplacian priors to convey the structure information of non-local similar patches, which is defined as

$$p(I) \propto \prod_{i=1}^{n} \exp\left(-\lambda_i \sigma(I_i)^{\gamma^i}\right) \tag{3}$$

where $I_i = [I_{i1}, I_{i2}, \ldots, I_{iN}] \in R^{n\times N}$ denotes i-th cluster of similar image patches extracted from the image I. n is the group number. λ_i is a positive tuning parameter and $\gamma^i (0 < \gamma^i < 1)$ denotes imposing the l_γ-norm-based constraint on the distribution of singular values of non-local similar patches.

To make it clearer, we study the negative logarithm of $p(I)$ which can be written as

$$\mathrm{R}(\sigma(I_i)) \triangleq -\log p(I) = \sum_i \lambda_i \|\sigma(I_i)\|^{\gamma^i}. \tag{4}$$

That is, $\mathrm{R}(\sigma(I_i))$ can be viewed as the deterministic regularization on the distribution of singular values.

With the constraint of the intrinsic structure sparsity of non-local patches, we present the following blind image deblurring model:

$$\begin{aligned}\left\{\hat{I}, \hat{k}\right\} = \arg\min_{I,k} \|I \otimes k - B\|_2^2 + \eta \|k\|_2^2 \\ +\mu \sum_i \lambda_i \|\sigma(I_i)\|^{\gamma^i} \\ + \sum_i \left(\tau \|R_i I - L_i\|_F^2 + \rho \|L_i\|_{\omega,*}\right),\end{aligned} \tag{5}$$

where L_i denotes the restored image patches with low rank property, R_i is the operation matrix of the i-th cluster, μ and τ are the regularization parameters for structured sparsity and low-rank constraints of similar non-local patches, respectively. η and ρ are weight parameters. The second term is the constraint which makes the blur kernel k to be stable. Compared with conventional LRMA algorithm, the proposed deblurring framework has two prominent advantages. On one hand, hyper-Laplacian regularization could facilitate to faithfully preserve the structural characteristics of the constructed matrix, leading to better deblurring result. On the other hand, adding hyper-Laplacian regularization to low rank representation model can further improve the local information preserving ability of model, which enables the model to better recover image components with low-rank properties.

IV. OPTIMIZATION

Due to the difficulty to estimate multiple variables directly of (5), we adopt the alternating minimization algorithm and split the energy function into two subproblems. That is, intermediate latent images and blur kernels can be obtained by separately, solving two subproblems as follows,

$$\begin{aligned}\hat{I} = \arg\min_I \|I \otimes k - B\|_2^2 + \mu \sum_i \lambda_i \|\sigma(I_i)\|^{\gamma^i} \\ + \sum_i \left(\tau \|R_i I - L_i\|_F^2 + \rho \|L_i\|_{\omega,*}\right),\end{aligned} \tag{6}$$

and

$$\hat{k} = \arg\min_k \|I \otimes k - B\|_2^2 + \eta \|k\|_2^2. \tag{7}$$

In the following, we further present an effective optimization scheme about these two subproblems.

A. ESTIMATE LATENT IMAGE I

In this subproblem, half-quadratic splitting technique [12] is adopted to solve non-convex minimization problem (6). We fix the blur kernel k and introduce an auxiliary variable G_i, then (6) can be reformulated as,

$$\begin{aligned}\hat{I} = \arg\min_I \|I \otimes k - B\|_2^2 + \zeta \sum_i \|P_i I - G_i\|_2^2 \\ +\mu \sum_i \lambda_i \|\sigma(G_i)\|^{\gamma_i} + \sum_i \left(\tau \|R_i I - L_i\|_F^2 + \rho \|L_i\|_{\omega,*}\right),\end{aligned} \tag{8}$$

where ζ is penalty parameter. P_i is the linear operator to extract non-local similar patches at location i from image I.

The above optimization problem (8) can be solved by optimizing I, G_i, L_i alternatively while fixing others. For the fixed G_i and L_i, we can obtain I by minimizing,

$$\begin{aligned}\hat{I} = \arg\min_I \|I \otimes k - B\|_2^2 + \zeta \sum_i \|P_i I - G_i\|_2^2 \\ +\tau \sum_i \|R_i I - L_i\|_F^2.\end{aligned} \tag{9}$$

By introducing another auxiliary variable z for I, the minimization problem (9) can be equivalently written as follows,

$$\begin{aligned}\left\{\hat{I}, \hat{z}\right\} = \arg\min_{I,z} \|I \otimes k - B\|_2^2 + \zeta \sum_I \|P_i z - G_i\|_2^2 \\ +\tau \sum_i \|R_i z - L_i\|_F^2 + \beta \|I - z\|_2^2,\end{aligned} \tag{10}$$

where β is a positive penalty parameter. For (10), we alternatively update the I and z by,

$$\hat{I} = \arg\min_I \|I \otimes k - B\|_2^2 + \beta \|I - z\|_2^2, \tag{11}$$

and

$$\begin{aligned}\hat{z} = \arg\min_z \zeta \sum_i \|P_i z - G_i\|_2^2 + \tau \sum_i \|R_i z - L_i\|_F^2 \\ +\beta \|I - z\|_2^2.\end{aligned} \tag{12}$$

Both the (11) and (12) have a closed-form solution. In which I can be solved directly through well-known FFT (Fast Fourier Transform),

$$\hat{I} = \mathcal{F}^{-1} \frac{\overline{\mathcal{F}(k)}\mathcal{F}(B) + \beta \mathcal{F}(z)}{\overline{\mathcal{F}(k)}\mathcal{F}(k) + \beta}, \tag{13}$$

where $\mathcal{F}(\cdot)$ and $\mathcal{F}^{-1}(\cdot)$ denote the FFT and inverse FFT (Fast Fourier Transform), and $\overline{\mathcal{F}(\cdot)}$ denotes the complex

conjugate operator. Given I, we can easily obtain the closed-form solution of (12), i.e.,

$$\hat{z} = \frac{\zeta \sum_i P_i^T G_i + \tau \sum_i R_i^T L_i + \beta I}{\zeta \sum_i P_i^T P_i + \tau \sum_i R_i^T R_i + \beta}. \tag{14}$$

For a fixed I, the subproblems with respect to G_i and L_i can be updated separately by minimizing the following function:

$$\hat{G}_i = \arg\min_{G_i} \zeta \|P_i I - G_i\|_2^2 + \mu\lambda_i \|\sigma(G_i)\|^{\gamma_i}, \tag{15}$$

and

$$\hat{L}_i = \arg\min_{L_i} \tau \|R_i I - L_i\|_F^2 + \rho \|L_i\|_{\omega,*}. \tag{16}$$

Note that (15) is a non-convex l_γ-norm minimization problem. The solution of G_i can be derived from the generalized soft-thresholding (GST) algorithm according to [41], i.e.,

$$\begin{aligned}\hat{G}_i &= T_{\gamma^i}^{GST}(P_i I; \frac{\lambda_i}{\zeta}) \\ &= \begin{cases} 0, \text{ if } |P_i I| \le \tau_{\gamma^i}^{GST}(\frac{\lambda_i}{\zeta})) \\ \text{sgn}(P_i I) S_{\gamma^i}^{GST}(|P_i I|; \frac{\lambda_i}{\zeta})), \text{ if } |P_i I| > \tau_{\gamma^i}^{GST}(\frac{\lambda_i}{\zeta})) \end{cases}\end{aligned} \tag{17}$$

where $S_{\gamma^i}^{GST}(|P_i I|; \lambda_i/\zeta)$ can be obtained by theorem 1 in [41]. Let $\lambda = \lambda_i/\zeta$, the thresholding value $\tau_{\gamma^i}^{GST}(\lambda)$ is

$$\tau_{\gamma^i}^{GST}(\lambda) = (2\lambda(1-\gamma^i))^{\frac{1}{2-\gamma^i}} + \lambda\gamma^i(2\lambda(1-\gamma^i))^{\frac{\gamma^i-1}{2-\gamma^i}}. \tag{18}$$

As for (16), apparently, it is a low-rank matrix approximation problem which has a closed-form solution, and can be optimized by the WNNM method in [38].

B. ESTIMATE BLUR KERNEL K

With I known, estimating k becomes a least squares problem. We solve the blur kernel k by adopting the fast deblurring method from [23] in gradient domain. Thus, equation (7) can be modified as

$$\hat{k} = \arg\min_k \|\nabla I \otimes k - \nabla B\|_2^2 + \eta \|k\|_2^2. \tag{19}$$

Then, the closed-form solution of k can be solved by FFT method,

$$\hat{k} = \mathcal{F}^{-1}\left(\frac{\overline{\mathcal{F}(\nabla I)}\mathcal{F}(\nabla B)}{\overline{\mathcal{F}(\nabla I)}\mathcal{F}(\nabla B) + \eta}\right). \tag{20}$$

Finally, k can be obtained by the inverse transform. After that, we regularize k to ensure it satisfies the constraints that elements of k are nonnegative and the sum of all elements is equal to 1. Similar to the state-of-the-art methods [12], [40], we use the coarse-to-fine strategy with an image pyramid for kernel estimation. The main steps of our deblurring algorithm are shown in Algorithm 1.

C. FINAL LATENT IMAGE ESTIMATION

Once the blur kernel k is obtained, it will be transformed into a non-blind deconvolution problem. A number of non-blind deconvolution methods can be used to restore the final sharp result. In this paper, we employ the non-blind deblurring algorithm from [15] to recover the final latent image.

Algorithm 1 Our Deblurring Algorithm

Input: Blurry image B
generate the initial blur kernel k.
for $j = 1, 2, \ldots, Iter$ **do**
$I \leftarrow B$, $\zeta \leftarrow 2\mu$.
Constructing non-local matrix $\{I_i\}_{i=1}^n$ from an initial I: partitioning the non-local similar patches into clusters via k-NN;
Conducting parameter estimation for each cluster.
for $i = 1, 2, \ldots, n$ **do**
solve G_i by minimizing (15)
solve L_i by minimizing (16).
end for
repeat
solve z by minimizing (12).
solve I by minimizing (11).
$\zeta \leftarrow 2\zeta$.
until $\zeta > \zeta_{max}$.
solve the blur kernel k by minimizing (19).
$\mu \leftarrow 0.9\mu$, $\tau \leftarrow 0.9\tau$.
end for
Output: Intermediate latent image I and blur kernel k.

V. EXTENSION TO NON-UNIFORM DEBLURRING

Our model can be directly extended to non-uniform deblurring. Previous studies have confirmed that images, which caused by camera shake, are mostly non-uniform blurry. Based on the geometric model of camera motion [33], [36], a non-uniform blurry image can be represented as a mixture of a set of projectively transformations of $\mathbf{I}$:

$$\mathbf{B} = \sum_t k_t \mathbf{h}_t \mathbf{I} + \mathbf{n}, \tag{21}$$

where $\mathbf{B}$, $\mathbf{I}$ and $\mathbf{n}$ denote blurry image, sharp image and possible noise in vector form, respectively; t is the index of camera trajectory, and k_t serves as the corresponding weight of the t-th camera pose; $\mathbf{h}_t$ denotes a transformation matrix which applies the t-th camera motion to the sharp image $\mathbf{I}$. According to [44], equation (21) can be reconstructed as

$$\mathbf{B} = \mathbf{H}\mathbf{I} + \mathbf{n} = \mathbf{A}\mathbf{k} + \mathbf{n}, \tag{22}$$

where $\mathbf{H} = \sum_t k_t \mathbf{h}_t$, $\mathbf{A} = [\mathbf{H}_1\mathbf{I}, \mathbf{H}_2\mathbf{I}, \ldots, \mathbf{H}_t\mathbf{I}]$ and $\mathbf{k} = [k_1, k_1, \ldots, k_t]^{\mathrm{T}}$. Based on (22), our non-uniform deblurring

problem is achieved by alternatively minimizing:

$$\hat{\mathbf{I}} = \arg\min_{\mathbf{I}} \|\mathbf{HI} - \mathbf{B}\|_2^2 + \mu \sum_i \lambda_i \|\sigma(\mathbf{I}_i)\|^{\gamma^i} + \sum_i \left(\tau \|R_i\mathbf{I} - \mathbf{L}_i\|_F^2 + \rho \|\mathbf{L}_i\|_{\omega,*}\right), \quad (23)$$

and

$$\hat{\mathbf{k}} = \arg\min_{\mathbf{k}} \|\mathbf{Ak} - \mathbf{B}\|_2^2 + \eta \|\mathbf{k}\|_2^2. \quad (24)$$

Similar to the strategies of optimizing uniform deblurring case, we introduce an auxiliary variable $\mathbf{G}_i$ and rewrite (23) as

$$\hat{\mathbf{I}} = \arg\min_{\mathbf{I}} \|\mathbf{HI} - \mathbf{B}\|_2^2 + \zeta \sum_i \|P_i\mathbf{I} - \mathbf{G}_i\|_2^2 + \mu \sum_i \lambda_i \|\sigma(\mathbf{G}_i)\|^{\gamma_i} + \sum_i \left(\tau \|R_i\mathbf{I} - \mathbf{L}_i\|_F^2 + \rho \|\mathbf{L}_i\|_{\omega,*}\right), \quad (25)$$

where $\mathbf{G}_i$ and $\mathbf{L}_i$ is the corresponding vector forms of G_i and L_i, respectively. Similar to (7), the optimization problem (25) can be solved by alternatively solving $\mathbf{I}$, $\mathbf{G}$ and $\mathbf{L}$. We use the same approach in (15) and (16) to optimize $\mathbf{G}_i$ and $\mathbf{L}_i$ by fixing $\mathbf{I}$. As for (24), the evolutionary process of the blur kernel is similar to the uniform deblurring case.

VI. EXPERIMENTAL RESULTS

In this section, we evaluate the proposed method on both synthetic and real blurred images and compare it to existing image deblurring algorithms. All the experiments are implemented with MATLAB. In all experiments, we empirically set $\mu = 0.005$, $\tau = 0.01$, $\rho = 0.01$, $\eta = 2$, $\beta = 0.025$, $\zeta_{\max} = 2$, and the number of iterations $Iter = 5$. The adaptive parameter estimation approach described in [35] is employed to estimate λ and γ. To give an assessment of the restored image quality, the Peak-Signal-to-Noise Ratios (PSNR) and the cumulative distributions of error ratio are used as the performance evaluation on kernel estimations and deblurred results.

A. EFFECTIVENESS OF PROPOSED PRIOR

As described in Sec. 3, our model relies on two regularized terms including heavy-tailed constraints of non-local singular values and low-rank constraints of non-local similar patches. Compared with the low-rank constraint term, the role of the heavy-tailed constraint of non-local singular values seems ambiguous. To better illustrate the effectiveness of each term, we separately remove the heavy-tailed constraint and low-rank constraint in the proposed method for comparisons. Fig. 2 shows the intermediate kernel estimating results of an image from kernel updating process which in the case of only using low-rank constraint and the case of only using heavy-tailed constraint and proposed method. As shown in Figs. 2(e)–(g), heavy-tailed constraint and low-rank constraint both facilitate kernel estimation. Especially, the proposed method is favorable to generate more reliable kernels. Fig. 2(b)–(d) shows the visual comparisons of final recovered images. As can be seen, the use of our method produces a clearer deblurred image, demonstrating the fact that the proposed method is valid by integrating constraints with low-rank property and heavy-tailed property.

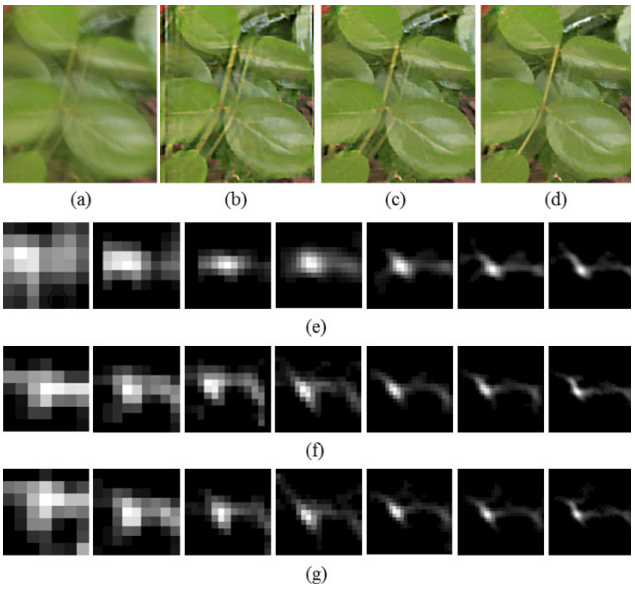

FIGURE 2. Comparisons of intermediate kernel estimating results and final deblurred results on an image. (a) is the blurry input. (b) and (c) are the deblurred results by using heavy-tailed constraint and using low-rank constraint, respectively. (d) is the deblurred result by our method. (e), (f) and (g) are the intermediate kernel results by using heavy-tailed constraint, low-rank constraint and our method, respectively. With our method, estimated kernel is more accurate and the final recovered image contains fewer artifacts.

B. EVALUATIONS ON SYNTHETIC DATASETS

To better demonstrate the effectiveness of our proposed method, we evaluate the proposed algorithm on two mainstream benchmark datasets [3], [42].

We first test on the dataset provided by Levin *et al.* [3], which contains 32 images from 4 original images with 8 uniform blur kernels. Direct calculation of PSNR may result in inaccurate results due to the relative conversion between ground-truth and deconvolution result. Therefore, error ratio is commonly used as performance evaluation for this dataset, which is proposed in [3], and it is defined as

$$R = \frac{\|I_e - I_g\|_2^2}{\|I_k - I_g\|_2^2}, \quad (26)$$

where I_e is the deblurred image with the estimated kernel, I_k is the deblurred image by with the ground-truth kernel, and I_g is the ground-truth clear image. The smaller R is, the better the reconstruction. The percentage of the results with error ratios below a threshold is defined as the success rate. As Fig. 3(a) shows, our proposed method performs competitively against other deblurring methods [1], [7], [12], [13], [15], [20] on this benchmark dataset [3]. Fig. 4 shows the deblurring results on two example images from this dataset, our method provides

TABLE 1. Comparison of PSNR (dB) and MSSIM values corresponding to the deblurring results in Fig. 5.

	[4]	[7]	[12]	[13]	[20]	[42]	Ours
PSNR	22.28	21.84	27.03	28.66	24.66	28.30	29.41
MSSIM	0.7617	0.7632	0.8358	0.8348	0.8157	0.8418	0.8420

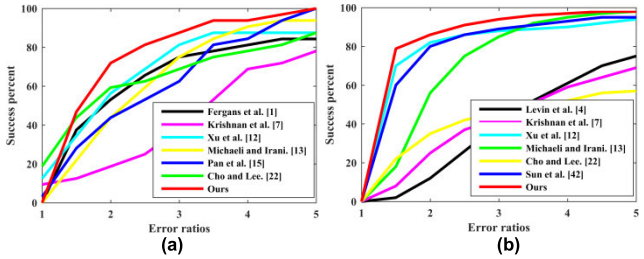

FIGURE 3. Quantitative evaluations on the benchmark datasets. (a) Levin *et al.* [3]. (b) Sun *et al.* [42].

the more reliable blur kernels with less noise. This is mainly because our prior can remove unfavorable details based on the low-rank attribute of non-local similar patches, which can better retain reliable information for kernel estimation.

Next, we evaluate our algorithm on the benchmark dataset by Sun *et al*. [42], which consists of 640 images generated by 80 high-resolution natural images of diverse scenes and 8 blur kernels from [3]. Six other state-of-the-art methods [4], [7], [12], [13], [20], [42] are choose for comparisons. Quantitative evaluations in terms of cumulative error ratio are shown in Fig. 3 (b). Note that the proposed method achieves favorably preformation against other approaches.

Visual comparisons of deblurring results obtained by the proposed algorithm and the state-of-the-art methods [4], [7], [12], [13], [20], [42] are shown in Fig. 5. The deblurred images by [4] and [7] suffer severe visual artifacts, and the estimated kernels are noisy. Although the deblurring methods by [13] [42] perform well on kernel estimation, they also generate some artifacts or encounter a degree of blur on the final deblurred images. In contrast, our method provides a reliable kernel and the recovered image is clearer with fewer artifacts. For a better comparison, Table 1 also shows the quantitative results of PSNR and the mean structural similarity index (MSSIM) corresponding to the deblurring results in Fig. 5, from which we can see that our method yields the highest PSNR and MSSIM values.

C. EVALUATIONS ON REAL IMAGES

We further evaluate our method on real dataset of Köhler *et al*. [43], which contains 12 space-varying blur kernels and 4 images. The PSNR is used to evaluate the performance. The result of each deblurred image was compared to 199 clear images captured along the camera motion trajectory, and the highest PSNR values were calculated. As shown in Fig. 6, the average PSNR value of the restored images by our method is higher than others. A visual comparison of an example with severe motion blur is shown in Fig. 7. The deblurred results of [7], [22] still contain severe motion blur, and the methods [21], [36] cannot restore visually acceptable images well, and the deblurring image of [2] contain ringing artifacts. Although the deblurring method [16] performs well, the dark pixels are too abrupt due to the dark channel prior. In contrast, our method generates more visual pleasing images. Table 2 shows that our method achieves the highest PSNR and MSSIM values in the deblurring results of Fig. 7.

(a) Blurred image (b) Krishnan et al. [7] (c) Xu et al. [12] (d) Cho and Lee [22] (e) Ours

FIGURE 4. Two examples on the synthetic blurred images from [3]. Our method generates better blur kernels compared to other methods.

TABLE 2. Comparison of PSNR (dB) and MSSIM values corresponding to the deblurring results in Fig. 7.

	[7]	[36]	[21]	[20]	[2]	[16]	Ours
PSNR	21.81	20.82	21.03	22.84	23.13	24.26	26.05
MSSIM	0.7407	0.6691	0.7388	0.7957	0.8106	0.8019	0.8280

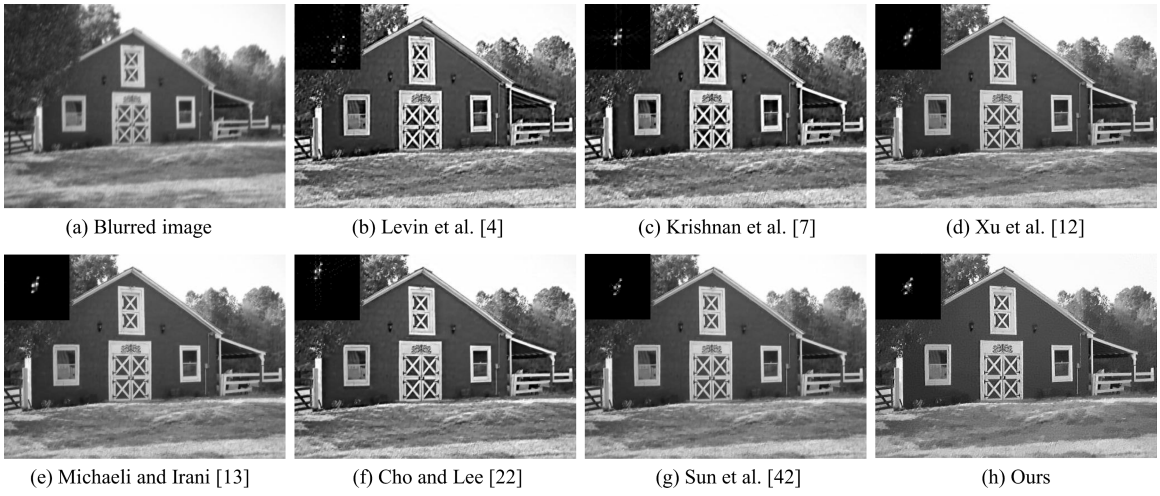

(a) Blurred image (b) Levin et al. [4] (c) Krishnan et al. [7] (d) Xu et al. [12]

(e) Michaeli and Irani [13] (f) Cho and Lee [22] (g) Sun et al. [42] (h) Ours

FIGURE 5. Deblurring results on an image from the dataset by Sun *et al.* [42]. Our recovered image has less ringing artifacts.

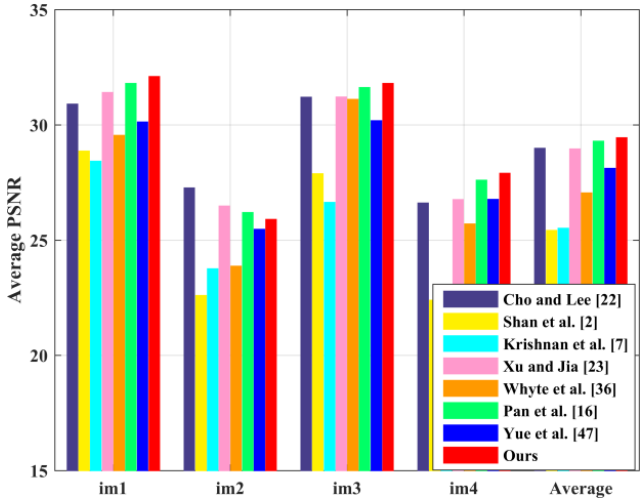

FIGURE 6. Quantitative comparison on Köhler dataset [43]. Our method overall outperform the compared methods.

In addition, we also use the real blurry images from [21] to test our method against two LRMA-based methods [17], [34]. Fig. 8 shows the deblurring results. As can be seen, the method [17] performs well on kernel estimation, but the deblurred results still contain some artifacts. Our method performs comparably to the method [34], which demonstrates the effectiveness of the proposed algorithm.

Fig. 9 shows the deblurred results on a real face image which contains few edges or texture. Compared with the state-of-the-art methods [7], [12], [17], [34], our algorithm generates the visually better result with sharp characters, and makes the edges of the clothes clearer and the face smoother. The implementation by Xu *et al.* [12] gets a poor deblurring result. The deblurred results by [7], [17], [34] contain varying degrees of artifacts.

D. NON-UNIFORM DEBLURRING

We also conduct experiments on two non-uniformly blurred examples, and compare the results with existing non-uniform methods [12], [16], [21], [29], [36]. As can be seen in Fig. 10 and Fig. 11, both of the compared methods perform well, but the regions inside green boxes are still a bit blurred. In contrast, the proposed method is able to remove blur and recover comparable and even better images with sharp edges.

E. ROBUSTNESS TO GAUSSIAN NOISE

Noise has a negative impact on the quality of blind image deblurring. In order to evaluate the robustness of our method to blurred image with noise, we manually blur an image with motion filter and add Gaussian noise with the mean value of 0 and the variance from 1 to 10 to an image. The deblurred results under different noise levels are shown in Fig. 12. Our algorithm performs well in the case of weak Gaussian noise, indicating that our method is robust to weak noise. This is mainly due to the robustness of non-local similar patches to weak noise. When the noise level reaches above 4, our method restores poor visual results and the estimated blur kernel is noisy. Recently, image denoising has been studied in depth as an independent branch. Separating the process of denoising and deblurring is beneficial to obtain better recovery results. In future work, we will consider developing the blind method that joint denoising and deblurring.

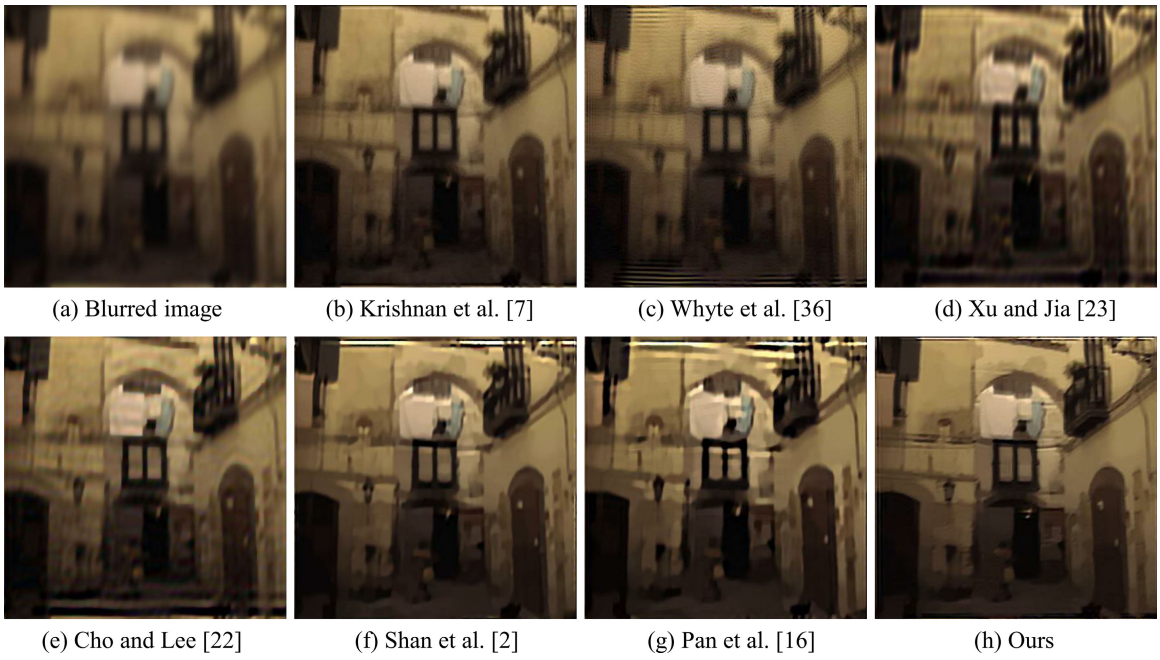

FIGURE 7. Deblurring results on an image from the dataset by Köhler *et al.* [43]. Our method produces more visual pleasing result.

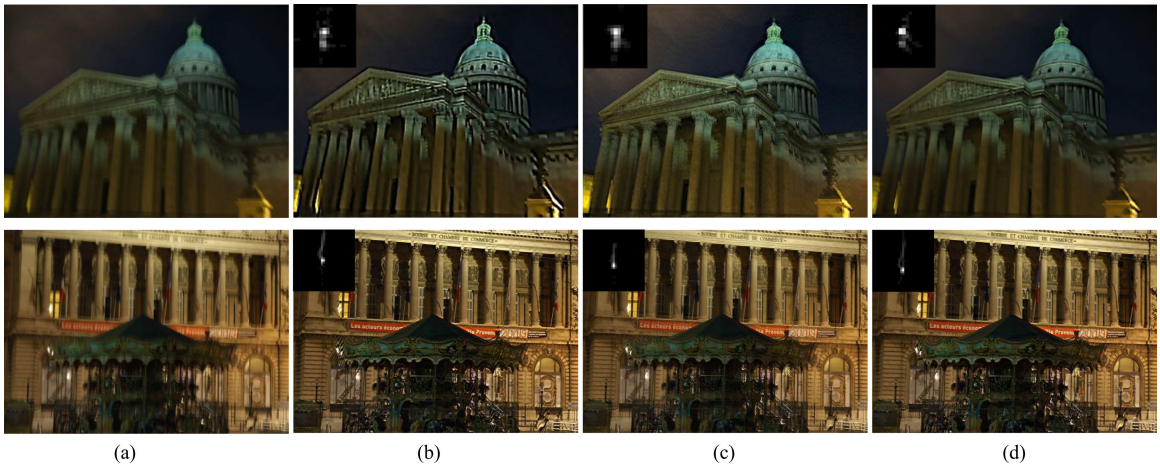

FIGURE 8. Visual comparison of two example images from [21]. (a) Blurry images. (b) Dong *et al.* [17]. (c) Ren *et al.* [34]. (d) Our results. Our method performs comparably, which demonstrates the effectiveness of the proposed algorithm.

FIGURE 9. Deblurred results on a real face image. The proposed method generates visually comparable result.

F. ANALYSIS OF COMPUTATIONAL COMPLEXITY

The computational complexity for iteration at each level mainly involves: 1) Searching similar patches via k-NN within a local window of size $W \times W$, while computational complexity of this step is $O(NP(W^2 + \log W^2))$, where N is the number of formed cluster by similar patches, and P is the number of similar patches. 2) The complexity of computing G_i and L_i is $O(NP^2h^2)$, where h is the patch

(a) Blurred image (b) Xu and Jia [23] (c) Pan et al. [16]

(d) Xu et al. [12] (e) Ours (f) Estimated kernels

FIGURE 10. Deblurring results on a non-uniform example with state-of-the-art non-uniform deblurring methods. Our method generates comparable results (best viewed on high-resolution display with zoom-in).

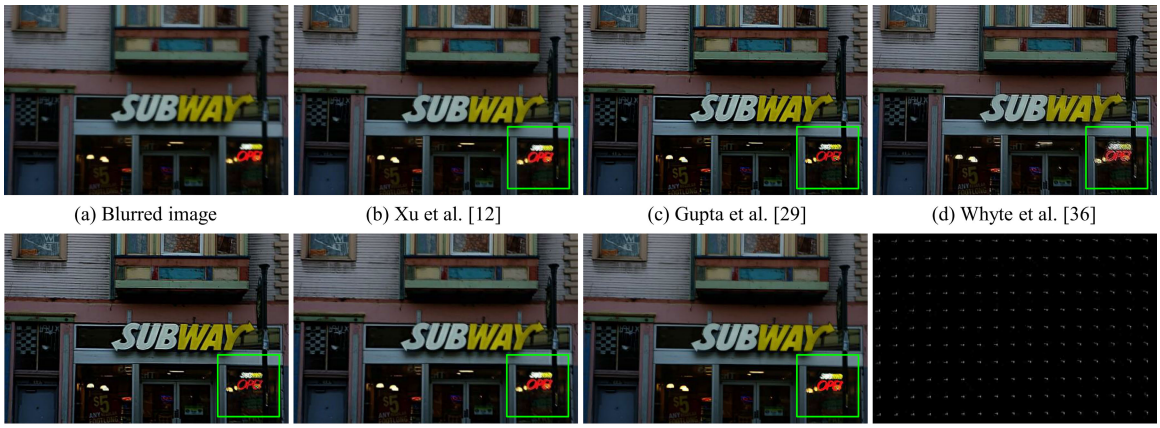

(a) Blurred image (b) Xu et al. [12] (c) Gupta et al. [29] (d) Whyte et al. [36]

(e) Xu and Jia [23] (f) Pan et al. [16] (g) Ours (h) Estimated kernels

FIGURE 11. Another non-uniform example with state-of-the-art non-uniform deblurring methods (best viewed on high-resolution display with zoom-in).

size. Hence, the overall computational complexity of our method is $O(NP(W^2 + \log W^2) + NP^2h^2)$. The other steps of Algorithm 1, such as computing z and I, can be accelerated by FFTs and inverse FFTs. Compared to the other methods [16] and [40], which have the computational complexity $O(M)$ and $O(h^2M)$ respectively, where M is the number of pixels, the proposed algorithm needs to search for similar patches and perform SVD operation, resulting in higher processing cost.

We also tested the running time of the iterative optimization process on blurred image with different sizes. Table 3 shows the time comparison of our method and other competing methods [7], [16]–[18], [34], on a computer with Intel Core i9-9940 CPU at 3.30 GHz. Our method is relatively time-consuming compared to methods of [7], [16], and [18]. However, compared to the methods [17] and [34], which also based on the low-rank prior, our method consumes much less time.

TABLE 3. Comparison of running time (in second). All methods are implemented in MATLAB.

Method	255×255	600×600	800×800
Krishnan et al. [7]	6.78	49.26	82.20
Pan et al. [16]	97.88	559.94	1180.20
Yan et al. [18]	9.98	63.92	126.77
Ren et al. [34]	358.71	1185.92	2621.18
Dong et al. [17]	342.73	2121.19	3701.50
Ours	140.21	791.64	1363.41

G. PARAMETER ANALYSIS

There are four main regularized weight parameters μ, τ, ρ, η in the model. We evaluate the impact of these weight parameter settings on the performance of our algorithm using dataset [3], and use kernel similarity criterion to quantitatively evaluate the accuracy of estimated kernel by

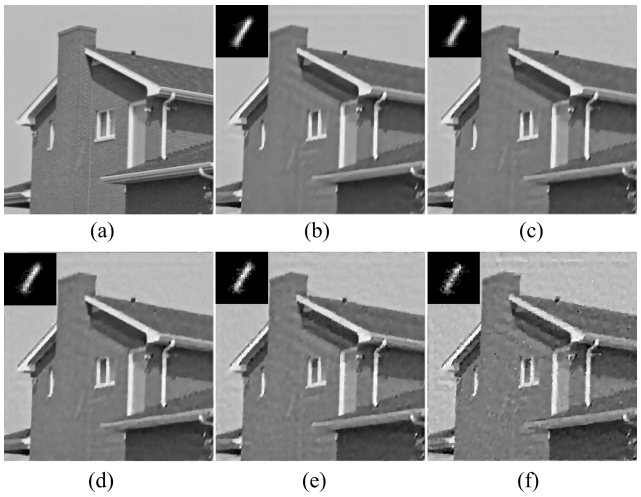

FIGURE 12. Deblurred results under gradual noise level. (a) Ground truth. (b) Gaussian noise variance is 1, PSNR: 28.11 dB. (c) Gaussian noise variance is 2, PSNR: 27.98 dB. (d) Gaussian noise variance is 3, PSNR: 27.18 dB. (e) Gaussian noise variance is 4, PSNR: 26.73 dB. (f) Gaussian noise variance is 5, PSNR: 25.06 dB.

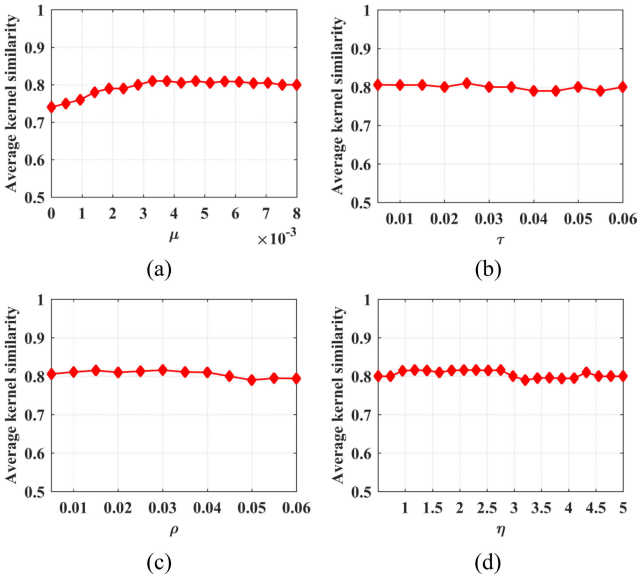

FIGURE 13. Sensitivity analysis of the main parameters μ, τ, ρ, and η in the proposed algorithm.

changing one parameter while fixing the other three parameters. As shown in Fig. 13(a)–(d), it has little effect on the algorithm when the regularization parameter changes within a reasonable range.

H. CONVERGENCE PROPERTY

As it includes several auxiliary variables during iterative optimization process due to the non-linear and non-convex of the proposed energy function, we analyze convergence properties of our method using images from the dataset of Levin *et al*. [3]. Fig. 14 (a) and (b) show the results in terms of energy referring to (5) and average kernel similarity [46] over iterations. Note that the proposed method converges well within 50 iterations, which demonstrates the effectiveness of our optimization scheme.

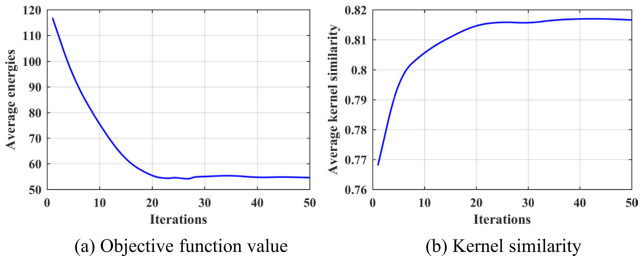

FIGURE 14. Convergence analysis of the proposed method. We evaluate the energy value referring to (5), and average kernel similarity over iterations.

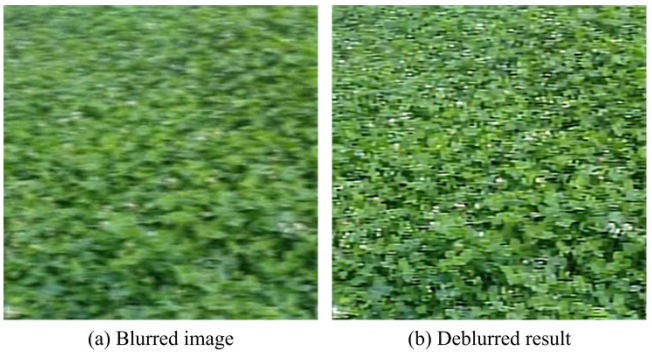

FIGURE 15. Limitation of the proposed model. Our method fails to restore the clear image due to the variety of rich textures.

I. LIMITATIONS

Although the proposed method performs well on a variety of datasets, it is less effective when a blurred image contains rich textures. In such cases, the property of non-local self-similarity does not hold due to the lack of non-local similar patches in the location of rich details. Fig. 15 shows a failure example of our method. As shown in Fig. 15 (b), the proposed method fails to restore the clear image and the restored image contains obvious ringing artifacts.

VII. CONCLUSION

In this work, we propose a novel method for blind image deblurring. The proposed method employs both heavy-tailed distribution of non-local singular values and low-rank characteristics of non-local similar patches. Heavy-tailed distribution is used to enforce intrinsic structure information while the low-rank prior is used to exploit the spatial sparsity.

To recover latent images, we develop an effective optimization scheme based on a half-quadratic splitting method. We also extend the method to handle non-uniform case. Evaluations on both synthetic and real images indicate that our method is effective in handling the blurred images and can produce comparable results, both visually and quantitatively.

REFERENCES

[1] R. Fergus, B. Singh, A. Hertzmann, S. T. Roweis, and W. T. Freeman, "Removing camera shake from a single photograph," *ACM Trans. Graph.*, vol. 25, no. 3, pp. 787–794, Jul. 2006.

[2] Q. Shan, J. Jia, and A. Agarwala, "High-quality motion deblurring from a single image," *ACM Trans. Graph.*, vol. 27, no. 3, p. 73, Aug. 2008.
[3] A. Levin, Y. Weiss, F. Durand, and W. T. Freeman, "Understanding and evaluating blind deconvolution algorithms," in *Proc. IEEE Conf. Comput. Vis. Pattern Recognit.*, Jun. 2009, pp. 1964–1971.
[4] A. Levin, Y. Weiss, F. Durand, and W. T. Freeman, "Efficient marginal likelihood optimization in blind deconvolution," in *Proc. IEEE Conf. Comput. Vis. Pattern Recognit.*, Jun. 2011, pp. 2657–2664.
[5] S. D. Babacan, R. Molina, and A. K. Katsaggelos, "Variational Bayesian blind deconvolution using a total variation prior," *IEEE Trans. Image Process.*, vol. 18, no. 1, pp. 12–26, Jan. 2009.
[6] D. Perrone and P. Favaro, "A clearer picture of total variation blind deconvolution," *IEEE Trans. Pattern Anal. Mach. Intell.*, vol. 38, no. 6, pp. 1041–1055, Jun. 2016.
[7] D. Krishnan, T. Tay, and R. Fergus, "Blind deconvolution using a normalized sparsity measure," in *Proc. IEEE Conf. Comput. Vis. Pattern Recognit.*, Jun. 2011, pp. 233–240.
[8] Y. Bai, G. Cheung, X. Liu, and W. Gao, "Graph-based blind image deblurring from a single photograph," *IEEE Trans. Image Process.*, vol. 28, no. 3, pp. 1404–1418, Mar. 2019.
[9] Z. Dou, K. Gao, X. Zhang, and H. Wang, "Fast blind image deblurring using smoothing-enhancing regularizer," *IEEE Access*, vol. 7, pp. 90904–90915, 2019.
[10] J.-F. Cai, H. Ji, C. Liu, and Z. Shen, "Framelet-based blind motion deblurring from a single image," *IEEE Trans. Image Process.*, vol. 21, no. 2, pp. 562–572, Feb. 2012.
[11] J.-F. Cai, E. J. Candès, and Z. Shen, "A singular value thresholding algorithm for matrix completion," *SIAM J. Optim.*, vol. 20, no. 4, pp. 1956–1982, Jan. 2010.
[12] L. Xu, S. Zheng, and J. Jia, "Unnatural l_0 sparse representation for natural image deblurring," in *Proc. IEEE Conf. Comput. Vis. Pattern Recognit.*, Jun. 2013, pp. 1107–1114.
[13] T. Michaeli and M. Irani, "Blind deblurring using internal patch recurrence," in *Proc. Eur. Conf. Comput. Vis.*, Zürich, Switzerland, Jun. 2014, pp. 783–798.
[14] J. Pan and Z. Su, "Fast l^0-regularized kernel estimation for robust motion deblurring," *IEEE Signal Process. Lett.*, vol. 20, no. 9, pp. 841–844, Sep. 2013.
[15] J. Pan, Z. Hu, Z. Su, and M.-H. Yang, "L_0-regularized intensity and gradient prior for deblurring text images and beyond," *IEEE Trans. Pattern Anal. Mach. Intell.*, vol. 39, no. 2, pp. 342–355, Feb. 2017.
[16] J. Pan, D. Sun, H. Pfister, and M.-H. Yang, "Blind image deblurring using dark channel prior," in *Proc. IEEE Conf. Comput. Vis. Pattern Recognit. (CVPR)*, Jun. 2016, pp. 1628–1636.
[17] J. Dong, J. Pan, and Z. Su, "Blur kernel estimation via salient edges and low rank prior for blind image deblurring," *Signal Process., Image Commun.*, vol. 58, pp. 134–145, Oct. 2017.
[18] Y. Yan, W. Ren, Y. Guo, R. Wang, and X. Cao, "Image deblurring via extreme channels prior," in *Proc. IEEE Conf. Comput. Vis. Pattern Recognit. (CVPR)*, Jul. 2017, pp. 4003–4011.
[19] N. Joshi, R. Szeliski, and D. J. Kriegman, "PSF estimation using sharp edge prediction," in *Proc. IEEE Conf. Comput. Vis. Pattern Recognit.*, Jun. 2008, pp. 1–8.
[20] J. Pan, R. Liu, Z. Su, and X. Gu, "Kernel estimation from salient structure for robust motion deblurring," *Signal Process., Image Commun.*, vol. 28, no. 9, pp. 1156–1170, Oct. 2013.
[21] D. Gong, M. Tan, Y. Zhang, A. Van Den Hengel, and Q. Shi, "Blind image deconvolution by automatic gradient activation," in *Proc. IEEE Conf. Comput. Vis. Pattern Recognit. (CVPR)*, Jun. 2016, pp. 1827–1836.
[22] S. Cho and S. Lee, "Fast motion deblurring," *ACM Trans. Graph.*, vol. 28, no. 5, p. 145, Dec. 2009.
[23] L. Xu and J. Jia, "Two-phase kernel estimation for robust motion deblurring," in *Proc. Eur. Conf. Comput. Vis.*, Sep. 2010, pp. 157–170.
[24] L. Yang and H. Ji, "A variational EM framework with adaptive edge selection for blind motion deblurring," in *Proc. IEEE/CVF Conf. Comput. Vis. Pattern Recognit. (CVPR)*, Jun. 2019, pp. 10159–10168.
[25] L. Li, J. Pan, W.-S. Lai, C. Gao, N. Sang, and M.-H. Yang, "Blind image deblurring via deep discriminative priors," *Int. J. Comput. Vis.*, vol. 127, no. 8, pp. 1025–1043, Jan. 2019.
[26] C. J. Schuler, M. Hirsch, S. Harmeling, and B. Scholkopf, "Learning to deblur," *IEEE Trans. Pattern Anal. Mach. Intell.*, vol. 38, no. 7, pp. 1439–1451, Jul. 2016.
[27] K.-H. Liu, C.-H. Yeh, J.-W. Chung, and C.-Y. Chang, "A motion deblur method based on multi-scale high frequency residual image learning," *IEEE Access*, vol. 8, pp. 66025–66036, 2020.
[28] X. Xu, J. Pan, Y.-J. Zhang, and M.-H. Yang, "Motion blur kernel estimation via deep learning," *IEEE Trans. Image Process.*, vol. 27, no. 1, pp. 194–205, Jan. 2018.
[29] Y. Liu, W. Dong, D. Gong, L. Zhang, and Q. Shi, "Deblurring natural image using super-Gaussian fields," in *Proc. 15th Eur. Conf. Comput. Vis.*, Sep. 2018, pp. 452–468.
[30] X. Cao, Y. Chen, Q. Zhao, D. Meng, Y. Wang, D. Wang, and Z. Xu, "Low-rank matrix factorization under general mixture noise distributions," in *Proc. IEEE Int. Conf. Comput. Vis. (ICCV)*, Dec. 2015, pp. 1493–1501.
[31] W. Dong, G. Shi, and X. Li, "Nonlocal image restoration with bilateral variance estimation: A low-rank approach," *IEEE Trans. Image Process.*, vol. 22, no. 2, pp. 700–711, Feb. 2013.
[32] L. Pan, R. Hartley, M. Liu, and Y. Dai, "Phase-only image based kernel estimation for single image blind deblurring," in *Proc. IEEE/CVF Conf. Comput. Vis. Pattern Recognit. (CVPR)*, Jun. 2019, pp. 6027–6036.
[33] Y.-W. Tai, P. Tan, and M. S. Brown, "Richardson-Lucy deblurring for scenes under a projective motion path," *IEEE Trans. Pattern Anal. Mach. Intell.*, vol. 33, no. 8, pp. 1603–1618, Aug. 2011.
[34] W. Ren, X. Cao, J. Pan, X. Guo, W. Zuo, and M.-H. Yang, "Image deblurring via enhanced low-rank prior," *IEEE Trans. Image Process.*, vol. 25, no. 7, pp. 3426–3437, Jul. 2016.
[35] S. Wang, L. Zhang, and Y. Liang, "Non-local spectral prior model for low-level vision," in *Proc. 11th Asian Conf. Comput. Vis.*, 2012, pp. 231–244.
[36] O. Whyte, J. Sivic, A. Zisserman, and J. Ponce, "Non-uniform deblurring for shaken images," *Int. J. Comput. Vis.*, vol. 98, no. 2, pp. 168–186, Jun. 2012.
[37] S. Gu, L. Zhang, W. Zuo, and X. Feng, "Weighted nuclear norm minimization with application to image denoising," in *Proc. IEEE Conf. Comput. Vis. Pattern Recognit.*, Jun. 2014, pp. 2862–2869.
[38] S. Gu, Q. Xie, D. Meng, W. Zuo, X. Feng, and L. Zhang, "Weighted nuclear norm minimization and its applications to low level vision," *Int. J. Comput. Vis.*, vol. 121, no. 2, pp. 183–208, Jan. 2017.
[39] Y. Zhou and N. Komodakis, "A map-estimation framework for blind deblurring using high-level edge priors," in *Proc. Eur. Conf. Comput. Vis.*, Jun. 2014, pp. 142–157.
[40] L. Chen, F. Fang, T. Wang, and G. Zhang, "Blind image deblurring with local maximum gradient prior," in *Proc. IEEE/CVF Conf. Comput. Vis. Pattern Recognit. (CVPR)*, Jun. 2019, pp. 1742–1750.
[41] W. Zuo, D. Meng, L. Zhang, X. Feng, and D. Zhang, "A generalized iterated shrinkage algorithm for non-convex sparse coding," in *Proc. IEEE Int. Conf. Comput. Vis.*, Dec. 2013, pp. 217–224.
[42] L. Sun, S. Cho, J. Wang, and J. Hays, "Edge-based blur kernel estimation using patch priors," in *Proc. IEEE Int. Conf. Comput. Photogr. (ICCP)*, Apr. 2013, pp. 1–8.
[43] R. Köhler, M. Hirsch, B. Mohler, B. Schölkopf, and S. Harmeling, "Recording and playback of camera shake: Benchmarking blind deconvolution with a real-world database," in *Proc. Eur. Conf. Comput. Vis.*, Oct. 2012, pp. 27–40.
[44] L. Zhong, S. Cho, D. Metaxas, S. Paris, and J. Wang, "Handling noise in single image deblurring using directional filters," in *Proc. IEEE Conf. Comput. Vis. Pattern Recognit.*, Jun. 2013, pp. 612–619.
[45] N. Komodakis and N. Paragios, "MRF-based blind image deconvolution," in *Proc. Asian Conf. Comput. Vis.*, 2013, pp. 361–374.
[46] Z. Hu and M.-H. Yang, "Good regions to deblur," in *Proc. Eur. Conf. Comput. Vis.*, Oct. 2012, pp. 59–72.
[47] T. Yue, S. Cho, J. Wang, and Q. Dai, "Hybrid image deblurring by fusing edge and power spectrum information," in *Proc. Eur. Conf. Comput. Vis.*, Jun. 2014, pp. 79–93.
[48] P. Qiu, "A nonparametric procedure for blind image deblurring," *Comput. Statist. Data Anal.*, vol. 52, no. 10, pp. 4828–4841, Jun. 2008.
[49] Y. Kang, P. S. Mukherjee, and P. Qiu, "Efficient blind image deblurring using nonparametric regression and local pixel clustering," *Technometrics*, vol. 60, no. 4, pp. 522–531, Jun. 2018.
[50] Y. Tang, Y. Xue, Y. Chen, and L. Zhou, "Blind deblurring with sparse representation via external patch priors," *Digit. Signal Process.*, vol. 78, pp. 322–331, Jul. 2018.
[51] Z. Xu, H. Chen, and Z. Li, "Blind image deblurring using group sparse representation," *Digit. Signal Process.*, vol. 102, Jul. 2020, Art. no. 102736.

[52] Z. Xu, H. Chen, and Z. Li, "Blind image deblurring via the weighted schatten p-norm minimization prior," *Circuits, Syst., Signal Process.*, to be published, doi: 10.1007/s00034-020-01457-z.
[53] Y. Guo and H. Ma, "Image blind deblurring using an adaptive patch prior," *Tsinghua Sci. Technol.*, vol. 24, no. 2, pp. 238–248, Apr. 2019.

XIAOLE CHEN received the B.S. degree in electronic science and technology from the North University of China, Taiyuan, in 2016, where she is currently pursuing the Ph.D. degree in instrument science and technology. Her research interests include image processing, machine learning (including deep learning), and its applications to computer vision tasks.

RUIFENG YANG received the B.S., M.S., and Ph.D. degrees in measurement technologies and instruments from the North University of China, Shanxi, in 1992, 1999, and 2005, respectively. From 2010 to 2012, he has studied with the Postdoctoral Center for Control Engineering, Beijing University of Aeronautics and Astronautics. He is currently a Professor with the School of Instrument and Electronics, North University of China, and the Director of the Automatic Test Equipment and System Engineering Research Center of Shanxi Province. His research interests include equipment test and system integration, automated testing and control, intelligent instruments, image processing, and machine vision.

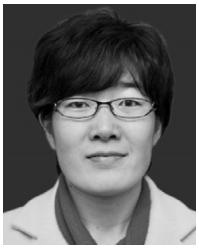

CHENXIA GUO received the B.S. degree in automation from the North University of China, Taiyuan, in 2001, the M.S. degree in test measurement technology and instrument, in 2006, and the Ph.D. degree in instrument science and technology from the North University of China, in 2014. She is currently an Associate Professor with the School of Instrument and Electronics, North University of China. Her research interests include visual measurement, automated testing and control, and complex electromechanical system design and integration.

SHUANGCHAO GE received the B.S. degree in electronic science and technology from Tianjin University, Tianjin, in 2009, the M.S. degree in solid geophysics from the Institute of China Seismological Bureau Crustal Stress, Beijing, in 2012, and the Ph.D. degree in earth exploration and information technology from the China University of Geosciences, Beijing, in 2016. Since 2016, she has been a Lecturer with the Department of Instrument and Electronics, North University of China. Her current research interests include data acquisition and processing, automated testing, and intelligent control.

ZHIHONG WU received the B.S. and M.S. degrees in measurement and control technology and equipment from the North University of China, Taiyuan, in 2017 and 2020, respectively, where he is currently pursuing the M.S. degree in instrumentation engineering. His research interests include automated test and control technology, vision-based control, and information fusion.

XIBIN LIU received the B.S. and M.S. degrees in electronic science and technology from the North University of China, Taiyuan, in 2014 and 2019, respectively. His research interests include image processing, and target recognition and tracking.